Remote Sensing of Environment 173 (2016) 109–121

Contents lists available at ScienceDirect

Remote Sensing of Environment

journal homepage: www.elsevier.com/locate/rse

Monitoring the river plume induced by heavy rainfall events in large, shallow, Lake Taihu using MODIS 250 m imagery

Yunlin Zhang [a,*], Kun Shi [a], Yongqiang Zhou [a,b], Xiaohan Liu [a,b], Boqiang Qin [a]

[a] Taihu Laboratory for Lake Ecosystem Research, State Key Laboratory of Lake Science and Environment, Nanjing Institute of Geography and Limnology, Chinese Academy of Sciences, Nanjing, China
[b] University of Chinese Academy of Sciences, Beijing, China

ARTICLE INFO

Article history:
Received 10 June 2015
Received in revised form 11 September 2015
Accepted 13 November 2015
Available online xxxx

Keywords:
Heavy rainfall event
Lake Taihu
MODIS
River plume
Total suspended matter

ABSTRACT

Knowledge of stormwater river plume dynamics is important for the management of lake water quality because river discharge associated with rainstorms can be a major source of pollutants for lake waters. Total suspended matter (TSM) derived from the discharge of sediment-laden rivers is highly variable over a wide range of time and space scales. In the present study, the first use of remote sensing to monitor the river TSM plume was conducted to investigate the effects of heavy rainfall events on Lake Taihu by the largest inflowing river (Tiaoxi River) based on a calibrated and validated model using daily 250 m MODIS imagery in band 1 (620–670 nm). From 2004 to 2013, 48 MODIS images of 20 heavy rainfall events were obtained, showing that the area of the TSM plume significantly increased in the waters adjacent to the inflowing river, reflecting runoff input. The TSM concentration of the river plume after heavy rainfall was significantly higher than that before rainfall (ANOVA, $p < 0.001$). A significantly positive correlation between the TSM plume area and the rainfall amount in heavy rainfall events ($p < 0.01$) was also observed. The heaviest rainfall event, in October 2013, caused a river plume with an area of 302.8 km^2, which lasted for more than 10 days. The significant increase in the frequency and rainfall amount of rainstorms and large rain in the past 50 years (1965–2014) in Lake Taihu under global warming indicated an important role of remote sensing in monitoring the river plume resulting from heavy precipitation. The present study demonstrates that remote sensing tools can be valuable instruments in the detection and tracking of the effect of heavy rainfall events on the distribution and diffusion of the TSM concentration in the lake. The results obtained from the present study are valuable for further hydrological research on the Tiaoxi River, particularly for the immediate assessment of flood impacts on soil erosion of the catchment.
© 2015 Elsevier Inc. All rights reserved.

1. Introduction

River plumes are the major route through which nutrients, sediments and other land-based pollutants, such as heavy metals and organic contaminants, are transported into lake waters (Qin, Xu, Wu, Luo, & Zhang, 2007; Rao & Schwab, 2007). Thus, river plumes play a fundamental role in the physical processes and biogeochemical cycles in lakes (White et al., 2009). The effects of river plumes on lake water quality and ecosystem structure and function can be considered from several aspects. (1) By inputting a large amount of nutrients from domestic, industrial and agricultural effluents, fluvial discharges modify the concentrations and ratios of nutrients in waters near the river mouth (Corcoran, Reifel, Jones, & Shipe, 2010). The over-enrichment of nutrients promotes phytoplankton growth, determines phytoplankton species distribution, and is detrimental to water quality (Grosse, Bombar, Doan, Nguyen, & Voss, 2010). (2) High concentrations of total suspended matter (TSM) and chromophoric dissolved organic matter (CDOM) discharged through the river plumes result in increased turbidity and decreased light penetration and submerged aquatic vegetation (SAV) growth (Cannizzaro, Carlson, Yarbro, & Hu, 2013; Ondrusek et al., 2012). (3) High concentrations of TSM, associated with bacteria and metallic pollutants and pesticides originating from industrial discharges and intensive agriculture or forestry plantations, affect lake water quality and human health (Kannan et al., 2012). (4) River plumes alter the nearshore thermal structure, and affect the vertical exchange of nutrients and the vertical migration of phytoplankton, zooplankton and fish (Rao & Schwab, 2007; Wang, Qian, Han, Luo, & Hamilton, 2012). Therefore, monitoring rainfall and overflows in rivers is important to determine their effects on water quality for sustainable lake management.

The effects of river plumes are best known for those caused by the high discharge following heavy rainfall (Chen, Huang, Chen, & Wang, 2011; Lahet & Stramski, 2010; Nezlin & DiGiacomo, 2005). However, these effects are typically limited when discharge is small. River plumes produced by stormwater discharge are easily distinguished from

* Corresponding author at: Yunlin Zhang, Nanjing Institute of Geography and Limnology, Chinese Academy of Sciences, 73 East Beijing Road, Nanjing 210008, China.
E-mail address: ylzhang@niglas.ac.cn (Y. Zhang).

http://dx.doi.org/10.1016/j.rse.2015.11.020
0034-4257/© 2015 Elsevier Inc. All rights reserved.

ambient coastal waters based on the high concentration of TSM that changes the color of the water surface. Although storm river plumes are typically studied using data collected from buoys and research vessels, the spatiotemporal variations of river plumes are typically too dynamic and broad; thus, these water bodies are not easily and effectively observed through shipboard monitoring (Nezlin, DiGiacomo, Stein, & Ackerman, 2005; Zawada et al., 2007). Another approach is to use hydrodynamic models in combination with estimated pollutant loads discharged from rivers to estimate the dispersal of pollutants (Hu, Jørgensen, & Zhang, 2006). However, this approach requires significant expertise and computational resources, and in most cases, the computed results have not been validated against in situ data.

Remote sensing technology overcomes the problems of conventional monitoring techniques and can be applied to the study of river plumes. Remote sensing using optical determination facilitates the identification of river plumes and provides a better understanding of TSM distribution and transport compared with conventional monitoring techniques. Although remote images seldom replace conventional sources of information for water resources, these images can supplement field data by revealing broad-scale patterns not recognizable at the surface, recording changes over time, providing data for inaccessible regions, and decreasing data acquisition costs (Lihan, Saitoh, Iida, Hirawake, & Iida, 2008; Warrick et al., 2007). However, a limitation of using remote sensing imagery is that cloud cover leads to missing data, and cloudiness is a common occurrence after a heavy rainfall (Petus et al., 2014).

Satellite imagery, including the Sea-Viewing Wide Field-of-View Sensor (SeaWiFS), Moderate Resolution Imaging Spectrometer (MODIS), Medium Resolution Imaging Spectrometer (MERIS), and Landsat Thematic Mapper (TM), has been widely used to monitor TSM transport and distribution from river plumes in estuarine and coastal waters (Guneroglu, Karsli, & Dihkan, 2013; Lahet & Stramski, 2010; Nezlin et al., 2005; Shen, Zhou, Li, He, & Verhoef, 2013). However, to our knowledge, there are few remote sensing studies on the effect of river plumes resulting from heavy rainfall on the transport and distribution of TSM in lakes (Binding, Greenberg, & Bukata, 2012; Lathrop, Vande Castle, & Lillesand, 1990). Typically, studies of river plumes in lakes are based on in situ measurement and numerical modeling (Churchill, Ralph, Cates, Budd, & Urban, 2003; He, Rao, Howell, & Skafel, 2006; McCullough & Barber, 2007; Pavlac et al., 2012; Rao & Schwab, 2007).

In Lake Taihu, the third largest freshwater lake in China, previous studies concerning the effects of temporal and spatial patterns on TSM concentration have used remote sensing estimation models (Sun et al., 2013; Wang, Shi, & Tang, 2011; Zhang, Shi, Liu, Zhou, & Qin, 2014). In these studies, attention is paid to the effects of lake topography, wind-driven sediment resuspension, and SAV distribution on TSM concentration (Zhang et al., 2014). However, there are no remote sensing studies associating the distribution of TSM concentration with river plumes and hydrological processes. This knowledge gap can be partially attributed to the lack of synchronous TSM distribution and hydrological and meteorological data and a failure to recognize the important role of river plumes in lake ecosystems due to the relatively low discharge of rivers flowing into lakes compared with the large discharge of rivers flowing into estuarine and coastal waters. For example, the Tiaoxi River, the largest inflowing river of Lake Taihu, has an annual inflow of 2.7 billion m^3 (Liu et al., 2011), which is substantially lower than some large rivers inflowing to the estuary and ocean (Bai et al., 2014; Petus et al., 2014; Thomas & Weatherbee, 2006).

To address this knowledge gap, in the present study, we present a methodological approach for monitoring the dispersion and effect of a river plume in a large shallow lake using remote sensing during heavy rainfall events. Specifically, the aims of the present study were to 1) quantify the areas and intensities of the river plumes for each heavy rainfall event from 2004 to 2013; 2) determine the persistence of the river plumes (i.e., determine how long the discharge signal is retained in the lake); and 3) determine the relationship between rainfall amount and TSM plume area using remote sensing.

2. Materials and methods

2.1. Study region

Lake Taihu, the third largest freshwater lake in China, has a complicated river and channel network, with 219 rivers or channels connecting to the lake (Qin et al., 2007). Most of the water enters the lake from west and flows out to the east, primarily through Eastern Taihu Bay. According to the inflow and outflow, the rivers associated with Lake Taihu are simplified to thirteen inflowing rivers in the western and northern areas and one outflowing river (Taipu River) in the eastern part of the lake (Fig. 1).

The Tiaoxi River exhibits the maximum inflow, and the associated river plume was the focus of the present study. The Tiaoxi River has an annual inflow of 2.7 billion m^3, contributing approximately 60% of the total water for Lake Taihu (Liu et al., 2011). The main stream of the Tiaoxi River is 158 km, and the catchment area is approximately 4576 km^2 with 90% vegetation cover. The width of the Tiaoxi River and average water depth are approximately 350 m and 2.5 m, respectively. The multi-year average precipitation amount of the Tiaoxi River catchment is approximately 1460 mm. Topography types of the catchment include hills (88%) and plains (12%). The upstream part of the river flows through agricultural areas, while the downstream part flows within the urban district of Huzhou and is subject to industrial inputs. The river collects waters from a population of approximately one million inhabitants, primarily located in moderately sized cities along the river continuum.

2.2. MODIS data and TSM estimation model

We used MODIS data to estimate the concentration of TSM in Lake Taihu. These data, available since 2002, have a spatial resolution of 250–1000 m. We used 250 m resolution MODIS imagery in band 1 (620–670 nm), which has been widely used to estimate TSM concentration or turbidity in diverse aquatic ecosystems (Chen, Hu, & Muller-Karger, 2007; Feng, Hu, Chen, & Song, 2014; Lahet & Stramski, 2010; Petus et al., 2010; Petus et al., 2014), and this technique is sufficiently accurate for Lake Taihu with a water area of 2338 km^2 (Shi et al., 2015; Wang et al., 2011). More importantly, the high frequency images (1/day) facilitated the monitoring of the turbid plume from the Tiaoxi River throughout heavy rainfalls. The MODIS-Aqua Level 1A data were obtained from NASA Goddard Space Flight Center and processed to Level 2 format using the NASA SeaWiFS Data Analysis System (SeaDAS version 5.1.6).

From January 2003 to December 2013, we set the criterion for matching the satellite data and the in situ observations to ≤3 h (the time interval between the in situ measurements and the corresponding MODIS-Aqua data) to produce 300 in situ TSM satellite-derived R_{rs} "matches", i.e., data pairs of MODIS-Aqua images represented by the same pixel. The 300 TSM satellite-derived *R*rs "matches" were randomly divided into calibration and validation datasets: 150 pairs were used to calibrate a TSM estimation model, and 150 pairs were used to validate the model. An empirical algorithm was calibrated and validated to estimate TSM concentration using MODIS band 1 in Lake Taihu based on the calibration and validation datasets (Fig. 2) (Shi et al., 2015). The detailed description including band optimization choice, atmospheric correction, model calibration and validation, and time series analysis of the TSM concentration from 2003 to 2013 has been previously elucidated (Shi et al., 2015). Thus, in the present study, we focused on the effect of the river plume resulting from heavy rainfall events in Lake Taihu using the TSM estimation model.

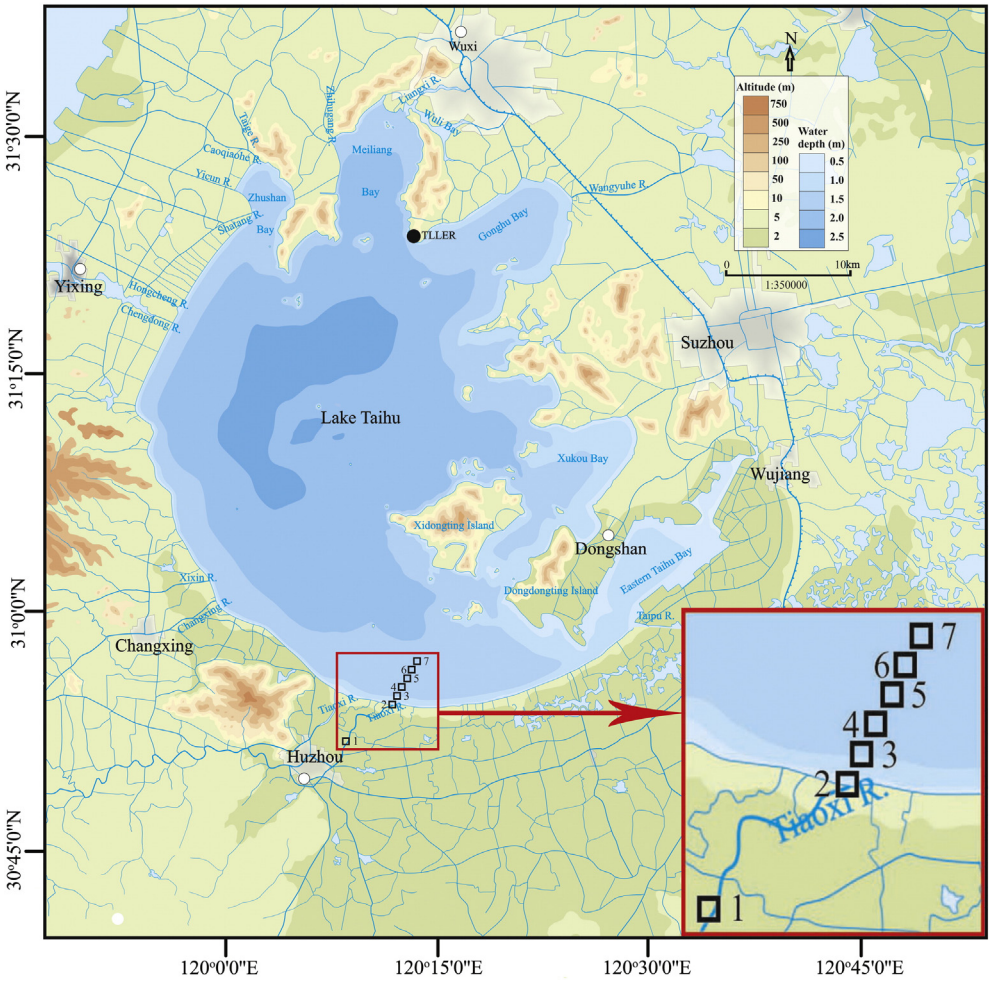

Fig. 1. Distribution of the 13 main inflowing rivers (the Tiaoxi River featured in this study flows into the south Lake Taihu) and the single outflowing river (Taipu River); (○) the Wuxi, Yixing, Donshan, and Huzhou meteorological stations, (●) TLLER water level observation station, and (□) sampling site on August 15 along the Tiaoxi River to the littoral zone after a heavy rainfall event from August 11 to 14, 2011.

2.3. Heavy rainfall events

For the present study, we selected the 20 heavy rainfall events from 2004 to 2013 resulting in marked river plume, determined through inspection of the MODIS images (Fig. 3). Generally, the rainfall events of more than 50 and 25 mm/day are considered rainstorms and large rain, respectively, according to the rainfall grade in China (Qian, Fu, & Yan, 2007). However, in Lake Taihu, marked river plume was still observed when the rainfall amount was near 20 mm. Therefore, in the present study, we defined a total rainfall amount of more than 20 mm as a heavy rainfall event. For each of the 20 heavy rainfall events, MODIS images were available for a day or days after the event, and for

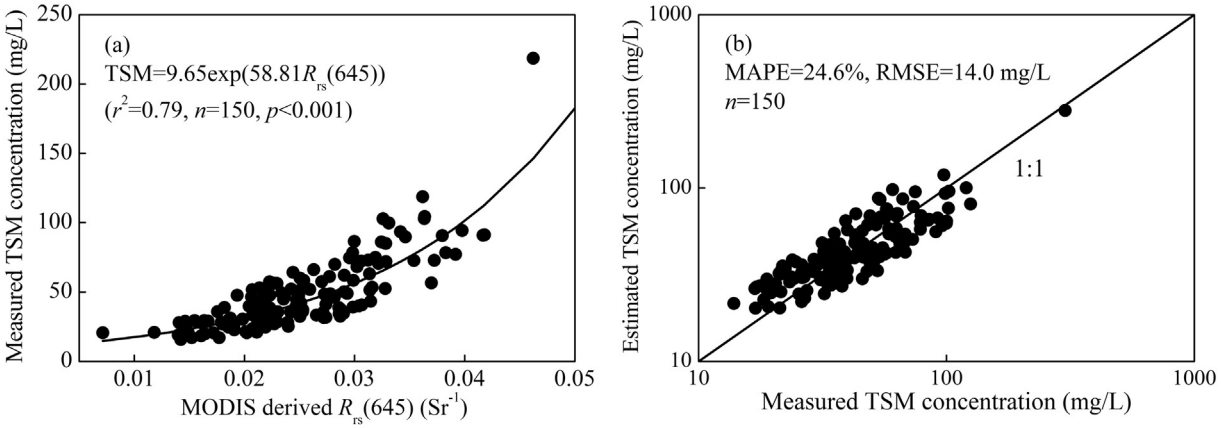

Fig. 2. Calibration (a) and validation (b) of a simple model to estimate the TSM concentration in turbid Lake Taihu using MODIS-Aqua remote sensing reflectance at 645 nm R_{rs}(645) derived by atmospheric correction (cited and revised from Shi et al., 2015).

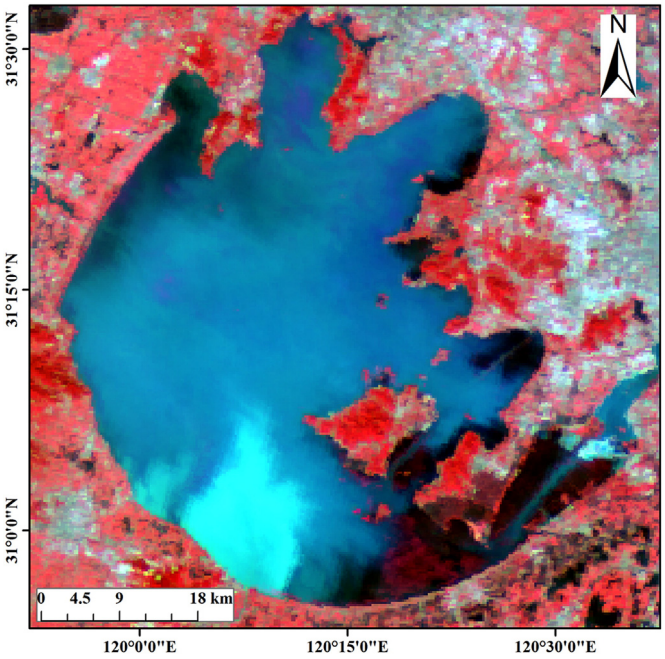

Fig. 3. MODIS imagery of the Tiaoxi River plume on 10 October 2013 (false color composite of $R_{rs}(859)$, $R_{rs}(645)$, and $R_{rs}(555)$).

14 of these events, MODIS images were also available for the day before the heavy rainfall. We collected a total of 48 MODIS images: 14 images before and 34 images after the heavy rainfall events (Table 1).

Daily rainfall data, representing the composite watershed, were collected at the Huzhou meteorological station (30.87° N, 120.05° E), in the suburb of Huzhou near the mouth of the Tiaoxi River (Fig. 1, ○). In addition, daily rainfall data from the four stations around Lake Taihu, including Huzhou, Dongshan (31.06° N, 120.43° E), Yixing (31.36° N, 119.81° E), and Wuxi (31.58° N, 120.32° E), were collected from 1965 to 2014 (Fig. 1, ○). The frequency and rainfall amount of rainstorms (≥50 mm/day) and large rain (≥25 mm/day) were calculated from 1965 to 2014 to analyze the long-term trend of heavy rainfall events in Lake Taihu. These data can be downloaded from the China Meteorological Data Sharing Service System (http://cdc.cma.gov.cn/home.do). The total rainfall amount for each heavy rainfall event was calculated as the sum of the rainfall amount for each of the individual days in the heavy rainfall event. We also obtained the daily wind speed and direction from the Huzhou meteorological station. To examine the strongest rainfall event during October 6–8, 2013, with a total rainfall amount of 306.5 mm, the daily water level data for October 2013 were obtained from the Taihu Laboratory for Lake Ecosystem Research (TLLER) on the shore of Meiliang Bay north of Lake Taihu (Fig. 1, ●).

Table 1
Beginning and end dates of 20 heavy rainfall events, accumulated rainfall amount determined from the daily total rainfall amount and the available MODIS imagery from 2004 to 2013 in Lake Taihu.

Event	Year	Beginning and end dates	Rainfall amount (mm)	Available MODIS imagery	
				Before heavy rainfall	After heavy rainfall
1	2004	24–25 June	82.7	22 June	27 June
2	2004	13–14 September	24.0	–	16–17 September
3	2005	19–20 July	53.9	–	23–24 July
4	2005	11–12 September	48.1	10 September	13, 17 September
5	2006	23–25 July	51.1	-	28–29 July
6	2007	14–16 March	70.7	13 March	20 March
7	2007	7–8 October	184.7	4 October	10–11 October
8	2008	9–11 June	92.5	5 June	12 June
9	2008	6–8 November	70.7	4 November	10, 13 November
10	2009	4–5 April	30.0	1 April	6, 8 April
11	2010	11–14 April	48.8	9 April	16 April
12	2010	4–5 July	46.8	-	7 July
13	2010	11–14 October	48.4	9 October	16, 17 October
14	2011	4–7 June	65.7	3 June	8 June
15	2011	24–30 August	94.9	–	31 August, 2, 4 September
16	2012	8 May	68.8	5 May	11 May
17	2012	17–18 June	35.0	15 June	21 June
18	2012	7–10 August	272.4	–	14 August
19	2013	16–17 May	58.5	14 May	19 May
20	2013	6–8 October	306.5	4 October	10, 12, 14, 21, 23 October

2.4. TSM measurement after a heavy rainfall event

On August 15, 2011 after a heavy rainfall event (August 11–14), we measured the TSM concentration profile along the Tiaoxi River to the littoral water. A total of 7 sites were distributed from the River Tiaoxi (site 1) to the river mouth (site 2) and further to the littoral water (sites 3–7) (Fig. 1, □). The distance of site 1 to site 2 was approximately 5 km, and sites 2–7 were set at 1-km distance. Surface water samples were collected at a depth of 0.5 m and stored in 21 acid-washed bottles on ice at 4 °C while in the field. The samples were filtered through pre-combusted (450 °C for 4 h) and pre-weighed Whatman GF/F filters to collect TSM of nominal sizes greater than 0.7 μm. The samples were subsequently dried (105 °C for 4 h) and weighed to calculate the TSM concentration.

2.5. Plume area calculation

A spatial autocorrelation technique was used to identify the river plume area from the MODIS-derived TSM imagery. Spatial autocorrelation is the correlation among values of a single parameter reflecting relatively close locations, considering the spatial attributes of geographical objects to evaluate and describe their relationships and spatial patterns (Myint, Wentz, & Purkis, 2007). Spatial autocorrelation measures the extent to which the occurrence of one object/feature is influenced by similar objects/features in the neighboring area (Myint et al., 2007). For remote-sensed imagery data, spatial autocorrelation suggests dependency between the values of each pixel in neighboring or proximal locations due to underlying common factors (Murphy, Tolhurst, Chapman, & Underwood, 2008). Geary's C is a popular index used to measure spatial autocorrelation, involving the computation of squared differences of values of pixel neighbors, defined as (Geary, 1954; Murphy et al., 2008):

$$C = \frac{(N-1)\sum_i \sum_j w_{ij}(X_i - X_j)^2}{2W\sum_i (X_i - X^*)^2} \quad (1)$$

where C is Geary's index, N is the number of the pixel denoted by i and j (the number of pixels in a given window), X is the variables of interest (MODIS derived TSM in this study), X^* is the average of X, w_{ij} is a matrix of spatial weights ($w_{ij} = 1$ if pixels i and j are contiguous, $w_{ij} = 0$ otherwise), and W is the sum of w_{ij}. The value of Geary's C index is between 0 and 2. A value of 1 means no spatial autocorrelation, while values lower than 1 demonstrate increasing positive spatial autocorrelation, and values higher than 1 illustrate increasing negative spatial autocorrelation. The local Geary's C index could be used to identify areas of high variability between a single pixel and the neighboring pixels; thus, this index is useful for detecting edge areas between clusters and other areas with dissimilar neighboring values. Spatial autocorrelation with Geary's C index was used in the present study to determine the plume area for each selected MODIS-derived image. Three steps are

needed to derive the plume area from MODIS-derived TSM imagery: 1) generating Geary's *C* index image data for each selected MODIS-derived TSM image using Equation (1), 2) determining the plume area threshold based on the calculated Geary's *C* index, and 3) calculating the plume area. In the first step, Rook's Case (pixels on the top, bottom, left and right) was selected as the neighborhood rule to define the adjacent pixels to compare with the central pixel. The most critical task in deriving the plume area from MODIS-derived TSM images was to determine the threshold value in the generated Geary's *C* index imagery. It is subjective and arbitrary to use trial and error together with visual analysis to determine the threshold value. Instead, we used Geary's *C* index gradients and statistics to determine this critical value. A pixel gradient was defined as the Geary's *C* index difference from the adjacent pixels in a given $3 * 3$ window. We generated a histogram of the pixels in the gradient image, and the mode of the maximum gradient could be determined. The pixels associated with the mode could be used to derive the plume area from MODIS-derived TSM images, as the Geary's *C* index values at the plume-nonplume boundary should markedly change. For a MODIS-derived TSM image without a plume area, the spatial distribution of Geary's *C* index should be homogeneous.

This method was applied to all selected image series and performed well for most of the images. Instead of using a different Geary's *C* index critical value for each image, we pooled all Geary's *C* index critical values to calculate the average and standard deviation. The universal Geary's *C* index critical value was obtained as the average value minus twice the standard deviation (Hu et al., 2010). The average value of all selected Geary's *C* index images was 0.009, and the corresponding standard deviation was 0.0005. Thus, the universal Geary's *C* index threshold value was determined as 0.008 ($0.009–0.0005 \times 2 = 0.008$). In addition, the sensitivity analysis indicated that using thresholds of 0.008 and 0.01 results in nearly identical statistics and spatial-temporal patterns, but the former typically led to 2% to 8% larger plume area coverage. Thus, a threshold of 0.008 was used in the present study, indicating a strong correlation. According to this threshold value (>0.008), it is easy to derive the plume area from MODIS-derived TSM images (Fig. 4a). Notably, as shown in Fig. 4b, the lake boundary and the plume area were both derived using this threshold value. However, it is not a difficult task to separate the plume area from the lake boundary through visualization.

The maximum and average plume areas obtained from MODIS images were used to determine the correlation between rainfall amount and plume area. If the MODIS images were available for only one day after the heavy rainfall event, then the maximum plume area was equal to the average plume area. If MODIS images were available for multiple days after the heavy rainfall event, then the maximum plume area was selected, and the average plume area was calculated from all available images. The maximal and average TSM concentrations of the river plume were similarly obtained from MODIS data for every heavy rainfall event.

2.6. Statistical analysis

Statistical analyses, including calculations of the average, maximum, and minimum values and linear and non-linear regressions, were performed using SPSS 17.0 software (Statistical Program for Social Sciences). To investigate the relationships between variables, we performed correlation analyses using SPSS software. The differences in parameters were assessed using one-way ANOVA ($p < 0.05$). Significance was reported at $p < 0.05$.

3. Results

3.1. TSM concentration along the river profile

A heavy rainfall event from August 11 to 14, 2011 with an accumulated rainfall amount of 58.5 mm, occurred prior to sampling (Fig. 5a). Heavy rainfall generated a large input of TSM. The TSM concentration at sites 1 and 2 in the Tiaoxi River was as high as 186.1 and 175.8 mg/L, respectively. From site 2 at the river mouth to the littoral water, the TSM concentration gradually decreased from 175.8 mg/L to the lowest value of 45.9 mg/L at site 7, reflecting the sedimentation and dilution of the TSM surrounding the clear water. A significantly negative linear relationship was observed between the TSM concentration and the distance to the river mouth ($r^2 = 0.90$, $p < 0.005$) (Fig. 5b).

3.2. Variation in the river plume area

Among the 20 heavy rainfall events from 2004 to 2013, the river plume area formed by the Tiaoxi River ranged from 2.8–302.8 km^2, with an average area of 43.7 ± 70.7 km^2 (Table 2). Overall, the river plume area gradually increased with time after the rainfall as a result of diffusion. In each of the 10 heavy rainfall events for which MODIS images were obtained for the two subsequent days after the rainfall, the

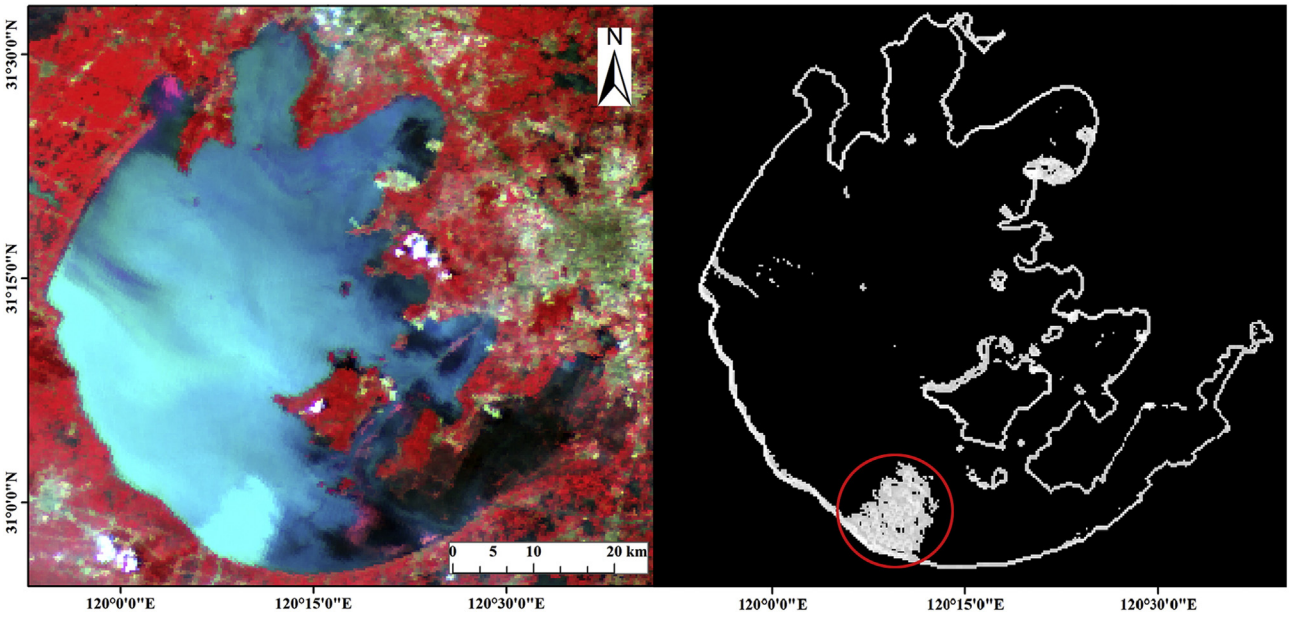

Fig. 4. MODIS-derived TSM image on July 24 (a) and the corresponding river plume from the Tiaoxi River using spatial autocorrelation (b).

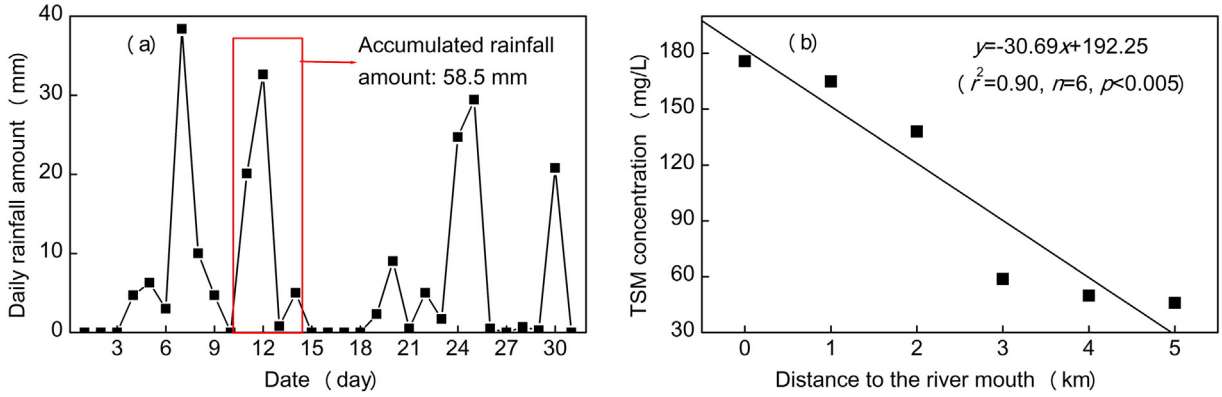

Fig. 5. Daily rainfall amount from August 1 to 31, 2011 (a) and the linear relationship between the TSM concentration and the distance to the river mouth (b). The red bar shows the heavy rainfall event from August 11 to 14, with accumulated rainfall of 58.5 mm prior to sampling.

river plume area markedly increased from 48.9 km^2, calculated from the first MODIS images, to 64.4 km^2, calculated from the second MODIS images. Other rivers entering Lake Taihu had either minimal or no plumes identified from the MODIS images, even after the 20 heavy rainfall events, reflecting the low discharge of these rivers. In addition, several inflowing rivers northwest of Lake Taihu flowed through the plain river network area before entering the lake (Fig. 1), resulting in decreased turbidity. Therefore, no marked river plume was observed in the MODIS images.

We characterized the plume features during the strongest rainfall event, October 6–8, 2013, with a total rainfall of 306.5 mm. During this event, the water level increased from 3.06 m on October 6 prior to the rainfall to a maximum of 3.77 m on October 13 after the rainfall, showing an increase in the water level of 0.71 m (Fig. 6). After excluding

Table 2
TSM concentration before rainfall, and the plume area and TSM concentration of the plume after heavy rainfall, for each of 20 heavy rainfall events from 2004 to 2013 in Lake Taihu.

Event	Year	Before rainfall	After heavy rainfall							
		TSM (mg/L)	Area (km^2)	TSM (mg/L)	Area (km^2)	TSM (mg/L)	Area (km^2)	TSM (mg/L)	Area (km^2)	TSM (mg/L)
1	2004	22 June	27 June							
		39.7	58.1	65.5	–	–	–	–	–	–
2	2004		16 September		17 September					
			6.2	101.4	18.7	242.4	–	–	–	–
3	2005		23 July		24 July					
			36	174.1	67.9	175.3	–	–	–	–
4	2005	10 September	13 September		17 September					
		34.3	5.1	132.5	17.1	84.1	–	–	–	–
5	2006		28 July		29 July					
			9.2	117.1	11.6	72.9	–	–	–	–
6	2007	13 March	20 March							
		45.0	49	129.1	–	–	–	–	–	–
7	2007	4 October	10 October		11 October					
		73.0	78	103.2	108	100.1	–	–	–	–
8	2008	5 June	12 June							
		90.5	50.2	312.0	–	–	–	–	–	–
9	2008	4 November	10 November		13 November					
		25.0	43.7	151.0	65	96.1	–	–	–	–
10	2009	1 April	6 April		8 April					
		55.8	2.8	79.0	6.3	86.5	–	–	–	–
11	2010	9 April	16 April							
		95.9	15.3	103.2	–	–	–	–	–	–
12	2010		7 July							
			30	194.8	–	–	–	–	–	–
13	2010	9 October	16 October		17 October					
		37.4	31.8	83.0	46.8	142.7	–	–	–	–
14	2011	3 June	8 June							
		21.3	31.6	54.6	–	–	–	–	–	–
15	2011		31 August		2 September		4 September			
			44	150.9	47.5	230.3	80	77.7	–	–
16	2012	5 May	11 May							
		29.6	15.7	140.0	–	–	–	–	–	–
17	2012	15 June	21 June							
		34.1	42.9	143.4	–	–	–	–	–	–
18	2012		14 August							
			244	148.2	–	–	–	–	–	–
19	2013	14 May	19 May							
		66.8	10.6	69.2	–	–	–	–	–	–
20	2013	4 October	10 October		12 October		14 October		21 October	
		62.8	232.5	127.5	255	119.3	270.3	111.9	302.8	73.3

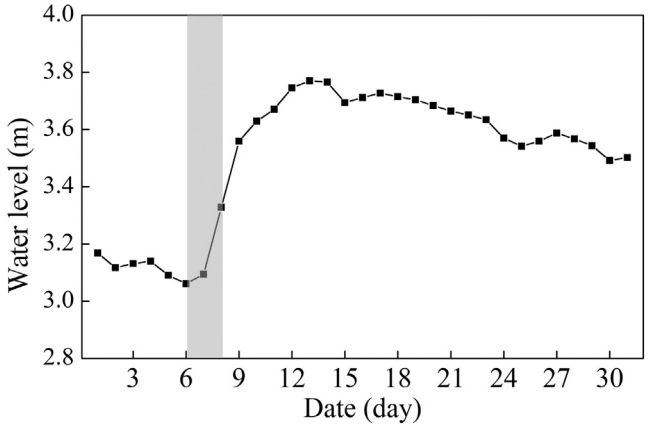

Fig. 6. Changes in the water levels of Lake Taihu from October 1 to 31 2013. The gray bar shows the strongest rainfall event from October 6–8, with a total rainfall amount of 306.5 mm.

a total rainfall amount of 306.5 mm, the river input from the catchment resulted in an increase of 0.40 m in the lake water level.

The formation and development of the river plume was shown in six MODIS images: one image before the event (October 4) and five images after the event (October 10, 12, 14, 21 and 23). On October 4, no river plume was distinguished in the MODIS image. On October 10, a marked river plume with an area of 232.5 km^2 was observed. On October 12, the fourth day after the end of the heavy rainfall, the river plume area increased to 255 km^2 through extension toward the north, driven by lake water currents resulting from southeasterly and south winds (Table S1). On October 14, the sixth day after the end of the heavy rainfall event, the river plume area increased to 270.3 km^2, with the plume from the Tiaoxi River combining with a small river plume formed by the adjacent Changxing River. On October 21, 13 days after the rainfall event, the river plume reached a maximal area of 302.8 km^2. On October 23, 15 days after the rainfall event, the river plume was still visible, although smaller, but the plume boundary was not easily identified, and the plume area was not calculated (Fig. 7).

There were highly significant linear correlations between (i) rainfall amount and maximum plume area and (ii) rainfall amount and average plume area (Fig. 8). When the correlation analysis was performed with exclusion of the three largest rainfall events with rainfall >120 mm (October 7–8, 2007; August 7–10, 2012; and October 6–8, 2013), significant linear relationships were still observed, indicating that the river plume area was controlled by the rainfall amount. The linear slope of the plume area vs. rainfall amount of all 20 rainfall events was close to that of the 17 events excluding the three largest rainfall events (0.96 vs 0.69 for maximal plume area and 0.89 vs 0.62 for average plume area) (Fig. 8). We further analyzed the plume area to rainfall ratio. For maximal plume area, the average ratios of plume area to rainfall were 0.65 ± 0.33 and 0.62 ± 0.35 km^2/mm, without statistical significance (ANOVA, $p = 0.79$), when including and excluding, respectively, the three largest rainfall events. Similarly, for the average plume area, the average ratios of plume area to rainfall were 0.58 ± 0.30 and 0.54 ± 0.30 km^2/mm, without statistical significance (ANOVA, $p = 0.76$), when including and excluding, respectively, the three largest rainfall events.

3.3. TSM concentration before and after heavy rainfall events: pooled data

Comparison of the TSM concentrations before and after heavy rainfall events showed that heavy rainfall had a significant impact on the concentration and distribution of TSM in the lake area adjacent to the Tiaoxi River (Table 2). For the 14 heavy rainfall events for which pre-rainfall MODIS images were available, the average pre-rainfall TSM concentration was 50.8 ± 23.9 mg/L, which was significantly lower than the maximum and average TSM concentrations of 125.7 ± 62.4 mg/L and 119.2 ± 62.0 mg/L, respectively, in the river plume after heavy rainfall (one-way ANOVA, $p < 0.001$).

During the 10 heavy rainfall events for which MODIS images were available for multiple days after the event, the TSM concentration exhibited different variation trends reflecting the balance between TSM input, sedimentation, dilution, and resuspension. In 5 of the 10 heavy rainfall events, the TSM concentration gradually decreased, reflecting the sedimentation and dilution of the TSM in the surrounding clear water. For example, from September 13–17 2005, the TSM concentration decreased from 132.5 to 84.1 mg/L, and from November 10–13 2008, the TSM concentration decreased from 151.0 to 96.1 mg/L (Table 2). In contrast, in 4 of the 10 heavy rainfall events, the TSM rapidly increased over time, reflecting continuous TSM input from the Tiaoxi River. For example, from September 16–17 2004, the TSM concentration increased from 101.4 to 242.4 mg/L, and from October 16–17 2010, the TSM concentration increased from 83.0 to 142.7 mg/L. In addition, in 2011, the TSM concentration increased from 150.9 mg/L on August 31 to 230.3 mg/L on September 2 and then rapidly decreased to 77.7 mg/L on September 4. The variations in TSM concentration after the heavy rainfall events reflect different controlling processes. In the initial 1–3 days, the TSM increased due to the input from the Tiaoxi River and then decreased in the late 5–7 days due to the sedimentation and dilution of the TSM in the surrounding clear water. Previous studies showed sediment resuspension and sedimentation were widely observed in the different lake regions in Lake Taihu (Liu, Zhang, Yin, Wang, & Qin, 2013; Qin, Hu, Gao, Luo, & Zhang, 2004; Zhang et al., 2006; Zhu et al., 2015). The critical wind speed of sediment suspension in Lake Taihu was 4.0 m/s. When the wind speed was lower than the critical wind speed, the TSM was suspended or settled in the water column (Qin et al., 2004). From September 1 to 4 in 2011, the daily average wind speed was 1.8, 1.8, 2.0, and 2.8 m/s (Table S1), indicating a marked TSM sedimentation in the water column, thereby decreasing the TSM concentration.

3.4. TSM concentration before and after the strongest rainfall event: October 6–8 2013

On October 4 before the strongest rainfall, the first MODIS image for this event showed that the average TSM concentration was 62.8 mg/L (Tables 1, 2 and Fig. 7). On October 10, two days after the event, the second MODIS image showed an average TSM concentration in the river plume of 127.5 mg/L, reflecting abundant input of TSM from the Tiaoxi River. On October 12 and 14, the fourth and sixth days after the end of the event, the average TSM concentration of the plume decreased to 119.3 and 111.9 mg/L, respectively. On October 21, 13 days after the rainfall event, the average TSM concentration in the plume was 73.3 mg/L, which was significantly higher than that of the water surrounding the plume. At 15 days after the strongest rainfall event, the river plume could still be observed in the MODIS image, although it was greatly diminished in intensity and size compared with that observed on October 10 (Fig. 7).

3.5. Correlation between rainfall amount and TSM concentration

The results showed that the rainfall amount was positively but not significantly associated with the maximum or average TSM concentrations of the river plume, which could be explained from three aspects. First, the availability of MODIS images after the heavy rainfall events was not consistent for all 20 heavy rainfall events. The MODIS images were occasionally available immediately or several days after the heavy rainfall event. Therefore, it is difficult to develop an empirical correlation between TSM concentration and rainfall amount for all 20 heavy rainfall events. Second, the TSM concentration in the Tiaoxi River resulting from the heavy rainfall events might have an upper limit value, depending on the vegetation cover, geology and geography

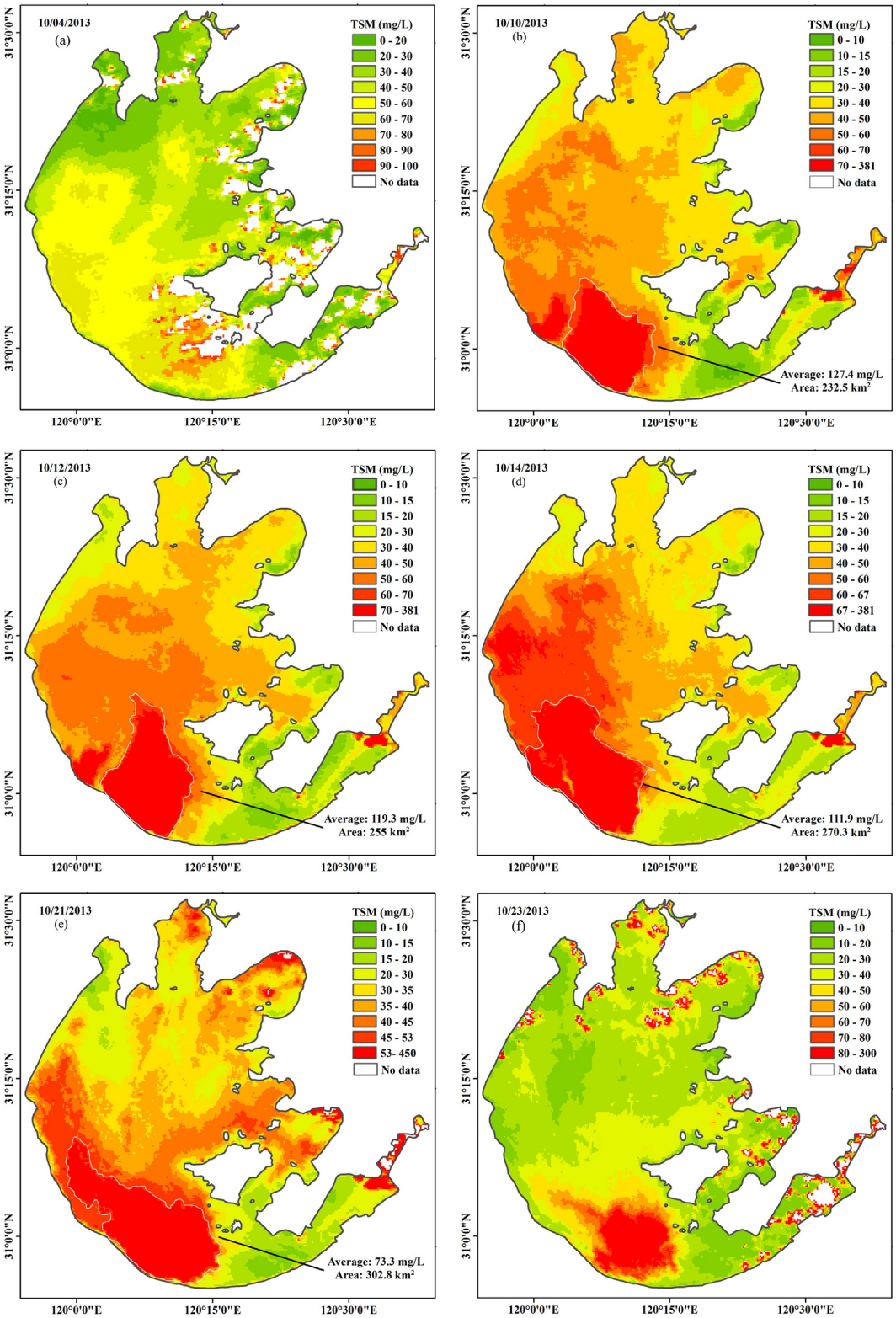

Fig. 7. TSM concentrations from MODIS mapping results before (a) and after (b-f) the heavy rainfall event of October 6–8, 2013. October 4, before (a); October 10, 2 days after (b); October 12, 4 days after (c); October 14, 6 days after (d); October 21, 13 days after (e); October 23, 15 days after (f). The outlined area represents the river plume.

conditions, and soil erosion intensity of the catchment. A total of 90% vegetation cover in the Tiaoxi River catchment causes the TSM concentration not to linearly increase with increasing rainfall amount. However, an increasing rainfall amount regulates the amount of sediment transported to the river, thereby increasing the TSM input into the lake without increasing the TSM concentration. Third, the rainfall amount was potentially not the only factor controlling the TSM concentration in the river plume. Other factors, such as background TSM concentration and sediment resuspension, might also control the TSM concentration in the river plume. The TSM concentration determined using the available MODIS images before the heavy rainfall event was significantly correlated with the daily average wind speed of the

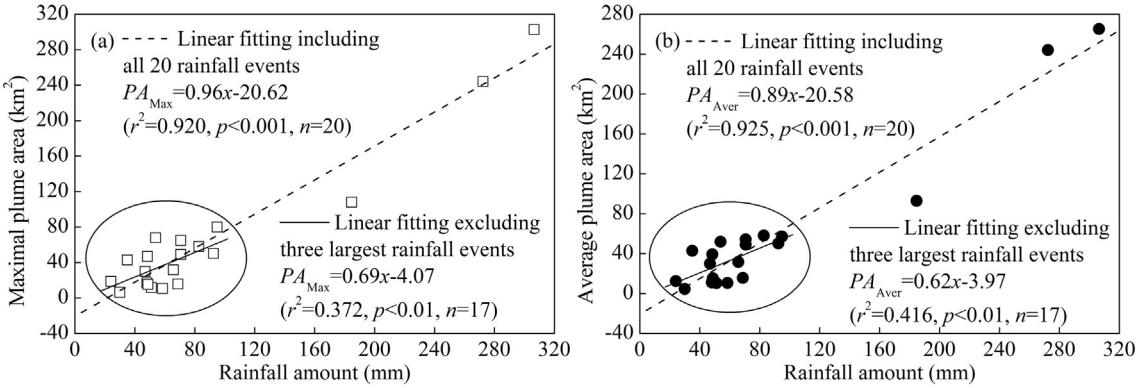

Fig. 8. Linear relationships between rainfall amount and maximal plume area (a) and average plume area (b).

antecedent day due to the lag of sediment resuspension induced by wind waves ($r^2 = 0.48$, $p < 0.01$, $n = 14$) (Fig. 9, Table S1), indicating the significant influence of wind waves on the TSM concentration. Therefore, the increase in the TSM concentration after the heavy rainfall event was not significantly positively correlated with the increase of rainfall in the river catchment.

4. Discussion

4.1. Application of remote sensing for tracing the river plume in lake turbidity

Due to the lack of in situ TSM concentration measurements in this region during heavy rainfall events, there is a clear need for more frequent and synoptic measurements of TSM to complement field data. Such data, obtained from satellite ocean color sensors, might facilitate the determination of the correlations between river input and lake ecosystem evolution to direct management efforts.

Currently, satellite imagery data are widely used to determine the distribution of environment parameters at large spatial scales, with better spatial and temporal resolution than that obtained using traditional measurement techniques. Previous studies using remote sensing imagery to study the spatio-temporal variability of river plumes have focused on the river plumes in estuary and coastal waters, discharged through relatively large river systems (Chen et al., 2011; Lahet & Stramski, 2010; White et al., 2009), based on 1-km resolution satellite data (Nezlin et al., 2005; Thomas & Weatherbee, 2006; Warrick et al., 2007). In the present study, we demonstrated the use of remote sensing to monitor the TSM plume resulting from heavy rainfall events in lake turbidity. The results showed that a linear model could be used to estimate the river plume area affected by heavy rainfall events when including and excluding the three largest rainfall events. In addition, the intercept of the relationships was small, suggesting that rainfall was the primary determinant of the river plume area.

The lack of larger scale spatial and temporal data for the Tiaoxi River plume has precluded in-depth analysis of the dynamics of the TSM plume. It is unlikely that traditional shipboard measurement can quantitatively determine the river plume area due to the constraints associated with field sampling (Corcoran et al., 2010). For example, in the Ventura region of the USA, the river plume areas obtained from satellite imagery significantly exceeded the areas covered using ship-based surveys, as station grids do not capture the entire regional plumes given the time, expense, and difficulty required from such an effort (Nezlin et al., 2008). We expect that these constraints also pertain to Lake Taihu, China, and that the areas of the Tiaoxi River plume, derived from the satellite images, exceed those determined using ship-based surveys. For large, shallow Lake Taihu, although there are comprehensive studies of a key determinant of TSM concentration, namely, the effect of wind-driven sediment resuspension (Zhang et al., 2006; Zhang et al., 2014), few studies have focused on the effect of river plume on the TSM concentration. Thus the application of remote sensing is of particular value. The present study demonstrates the advantageous application of remote sensing to obtain large spatial scale data on the TSM plume (compared with traditional shipboard in situ measurement)

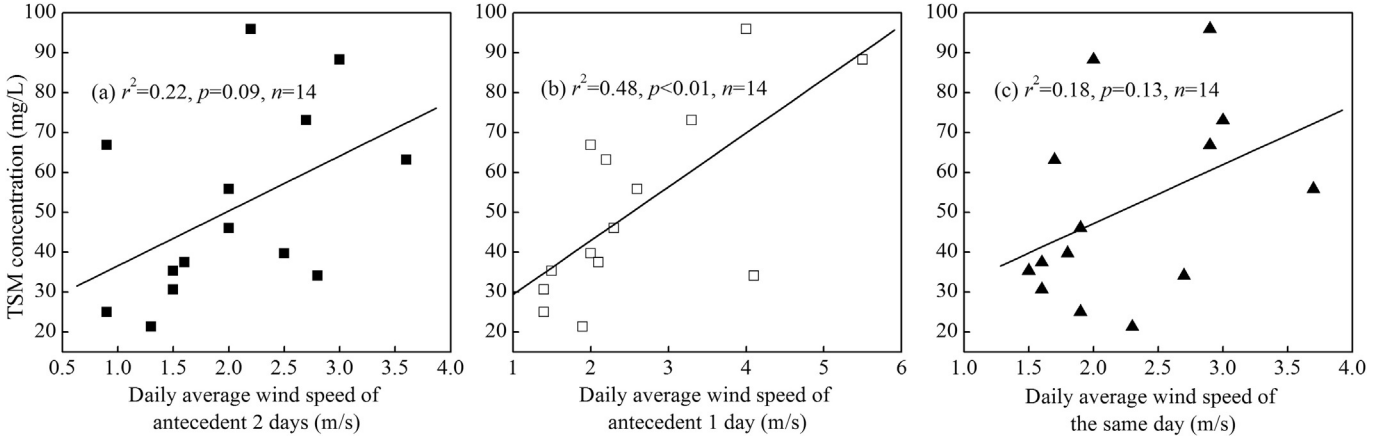

Fig. 9. Linear relationships between the TSM concentration and the daily average wind speed of the antecedent 2 days (a) and 1 day (b) and the same day (c) for the 14 available MODIS images obtained before the heavy rainfall.

and enhances the current knowledge of the important effects of heavy rainfall-induced river plumes on the TSM concentration in a large shallow lake.

However, describing the river plume using remote sensing technology has some limitations, particularly concerning the time series resulting from the relatively low revisit frequency for some satellites and cloudy weather (Petus et al., 2014; Svejkovsky, Nezlin, Mustain, & Kum, 2010). In the present study, images were not available and continuous for all days of interest associated with the heavy rainfall events. Heavy Tiaoxi River discharges are associated with stormy or windy conditions, characterized by high rainfall and extensive cloud coverage. These two factors prevent the collection of satellite images with information on water color and river plume turbidity. These images are available for the decreasing discharge periods following flood peaks, when cloud coverage decreases. From 2004 to 2013, only 48 cloud-free images were available for the 20 heavy rainfall events, accounting for only 20% of the 99 heavy rainfall events.

However, similar weather-related limitations also apply when using in situ measurements, as shipboard surveys and sampling data quality are highly dependent on the wind and lake conditions (Warrick et al., 2007). Thus, despite the monitoring system employed, there are challenges in describing the Tiaoxi River turbid plume during maximum flood events. Consequently, the maximum river plume and TSM concentration discharged through the Tiaoxi River turbid plume are likely underestimated.

Despite these limitations, the MODIS database used in the present study provided a frequent overview of the Tiaoxi River turbid plume, confirmed by our field observation after a heavy rainfall event from August 11 to 14, 2011. The satellite database was representative of all heavy rainfall events in Lake Taihu (Fig. 7), facilitating a description of the spatio-temporal variability in the river plume area affected by heavy rainfall events over multiple years. In the future, remote sensing will play an important role in monitoring the river plume resulting from heavy rainfall events because extreme precipitation and flood events are expected to increased based on the evidence of global warming and the anthropogenic influence on various aspects of the global hydrological cycle (O'Gorman & Schneider, 2009; Stocker, Dahe, & Plattner, 2013). For example, the Coupled Model Intercomparison Project Phase 5 (CMIP5) simulation projected an increase in the globally averaged 20-year return values of annual maximum 24-h precipitation amounts of approximately 6%/°C of global average warming (Kharin, Zwiers, Zhang, & Wehner, 2013). The past 50-year (1965–2014) observation of Lake Taihu showed that the frequency and rainfall amount of rainstorms and large rain significantly increased (Fig. 10), indicating an increase of heavy precipitation. The heavy rainfall events have been associated with strong soil erosion and loss and increased sediment loading to form the river plume to the lake from the catchment (Coppus & Imeson, 2002). In addition, this approach facilitates the immediate and effective evaluation of ecosystem conditions for ecosystem health assessment after severe flood events.

4.2. Spatio-temporal extent and affecting factors of the river plume

In the present study, the river plumes after heavy rainfall events in Lake Taihu markedly varied in size, and the largest extended up to 302.8 km^2, whereas the smallest was only 2.8 km^2 (Table 2, Fig. 7).

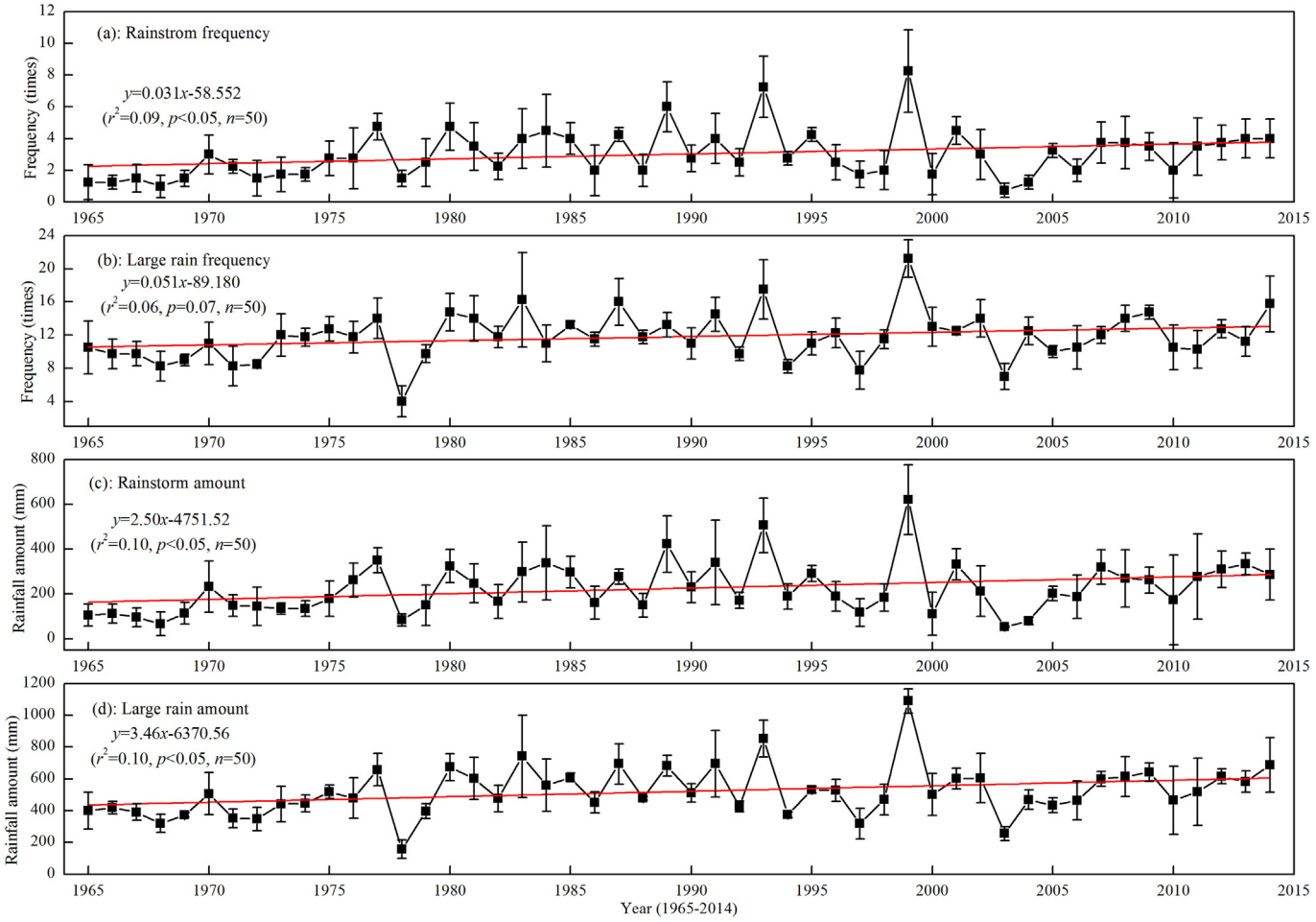

Fig. 10. Long-term trends in the frequency (a, b) and rainfall amount (c, d) of rainstorms and large rain from 1965 to 2014 in Lake Taihu. The red straight line indicates the linear fitting frequency and rainfall amount vs year. (For interpretation of the references to color in this figure legend, the reader is referred to the web version of this article.)

The duration of the river plumes ranged from 1 day to more than 10 days (October 9–23, 2013) (Table 2, Fig. 7). In addition, although the field investigation of the TSM concentration after a heavy rainfall event could not map the area of the river plume in the present study, the marked decrease in the TSM concentration from the mouth of the Tiaoxi River to the littoral water further confirmed that river input after heavy rainfall events could provide a large amount of TSM and form the potential high turbid region around the littoral water.

Although freshwater river discharge entering a freshwater lake exhibited different behaviors, including dispersion, dilution, and biogeochemical processes, compared with freshwater river discharge entering the estuary and ocean, the spatial extent and persistence of the river plumes resulting from heavy rainfall events documented in the present study in Lake Taihu were comparable to those of river plumes in other regions (Nezlin et al., 2005; Petus et al., 2010). The most common plume area in Santa Monica Bay, California (USA) was ~2 km^2, and the maximum plume area was 30–60 km^2, based on data obtained from the Sea-viewing Wide Field-of-view Sensor (SeaWiFS) between 1997 and 2003 (Nezlin et al., 2005). The river plumes persisted in Santa Monica Bay, California (USA) for at least 6 days (Corcoran et al., 2010). The Adour River turbid plume area (Bay of Biscay, France) ranged from less than 1 km^2 to more than 1500 km^2 based on MODIS 250 m imagery (Petus et al., 2010).

In estuary and coastal waters, spatio-temporal variations of river plumes are affected by many factors, including tide, rainfall, river discharge, wind, current, and extreme weather events (Chung, Liu, Chiu, & Liu, 2014; Lihan et al., 2008). However, in lake waters, the river plume area and spatio-temporal expansion are primarily controlled by rainfall, river discharge and wind. Many studies in lakes have shown that the amount of rainfall over the watershed was the main factor regulating the area of the river plume (Nezlin & DiGiacomo, 2005; Nezlin et al., 2005; Petus et al., 2010), consistent with the results of the present study. In Lake Taihu, both the maximal and average river plume areas significantly increased with increasing amounts of rainfall (Fig. 8). Similar correlations have been reported for southern California coastal waters in Orange County and San Diego regions (Nezlin & DiGiacomo, 2005; Nezlin et al., 2005). The amount of river discharge is typically proportional to the amount of rainfall (Chung et al., 2014), and thus, the amount of discharge similarly affects the river plume compared with the amount of rainfall. In the present study, we did not discuss the effect of river discharge because these data were not available.

The spatial variability of a river plume is greatly influenced by wind (Lahet & Stramski, 2010; Petus et al., 2010; Thomas & Weatherbee, 2006; Warrick et al., 2007), and wind is also a major factor controlling the transport pathways of the river plume (Lihan et al., 2008). In the present study, it was difficult to quantitatively describe the effect of wind speed on changes in the area of the river plume for each of the heavy rainfall events due to insufficient continuous available MODIS images. However, it was evident that in the strongest rainfall event, in October 2013, the expansion of the river plume from October 12 to 14 toward the northern and northwestern littoral regions, following the rainfall event of October 6–8, was affected by southeasterly and south winds from October 12 to 14 (Table S1).

In addition, sediment resuspension driven by wind significantly affected temporal changes in the TSM concentration of the river plume. The high daily average wind speeds of 5.4, 6.3, and 5.0 m/s on October 6, 7, and 8 (Table S1), which were markedly higher than the 4.0 m/s critical wind speed of sediment resuspension in Lake Taihu (Qin et al., 2004), caused sediment resuspension, contributing to the increase of the TSM concentration from 62.8 mg/L on October 4 to 127.5 mg/L on October 10. In contrast, the average TSM concentration of the river plume decreased to 119.3 and 111.9 mg/L on October 12 and 14, respectively, reflecting the dilution and sedimentation accompanying the low daily average wind speed from October 9 to 14 (1.2, 1.5, 2.5, 2.9, 3.1, and 2.9 m/s) (Table S1), which was markedly lower than the 4.0 m/s critical wind speed of sediment resuspension (Qin et al., 2004). Therefore, both the turbid river plumes and sediment resuspension driven by wind collectively produced the overall pattern of TSM concentration. Indeed, many previous studies have confirmed that sediment resuspension driven by wind waves significantly affected temporal changes in the TSM concentration in shallow Lake Taihu (Liu et al., 2013; Qin et al., 2004; Zhang et al., 2006).

4.3. Future improvements of the present study

In the present study, we demonstrated that remote sensing images yield valuable data in studies of the effects of the inflowing rivers on lake turbidity. However, further refinements are needed. Increasing the amount of satellite data should increase the number of ocean color data matching different heavy rainfall event conditions and increase the temporal representation of the satellite database. Images at higher temporal resolution (hourly rather than daily) are required to better characterize higher-scale phenomena, such as the continuous spread of the river plume in Lake Taihu after each heavy rainfall event. A potential source of such high temporal resolution data is the Geostationary Ocean Color Imager (GOCI) launched in June 2010 for the near real-time monitoring of aquatic environments in northeast Asia, with a 500 m spatial resolution that provides an accurate estimation of the TSM concentration (Choi et al., 2014; He et al., 2013). The GOCI covers Lake Taihu and is composed of sixteen (4×4) slot images, facilitating the hourly monitoring of the TSM concentration and the expansion of the river plume after heavy rainfall events in Lake Taihu.

To assess the exposure of lake ecosystems to land-based pollutants discharged through the Tiaoxi River, it would be necessary to scale the satellite-retrieved spatial and temporal information (such as the risk of exposure to lake ecosystems from the inflowing river waters) with in situ water quality measurements, such as loads of nutrients (which increase phytoplankton production), pollutants and bacteria (threatening ecosystem and human health). A study in Santa Monica Bay, California (USA) through shipboard monitoring showed that the waters of the river plume had higher concentrations of dissolved nitrogen and CDOM compared with the surrounding waters, leading to increases in diatom biomass and primary productivity (Corcoran et al., 2010). In the present study of Lake Taihu, we showed that the turbid plume of the Tiaoxi River had a significant effect on the TSM concentration and nutrient input, which certainly will have an important effect on the underwater light climate in the southwestern part of Lake Taihu because the TSM concentration is the determining factor of the underwater climate in Lake Taihu (Liu et al., 2013; Zhang, Zhang, Ma, Feng, & Le, 2007). Therefore, the scarce distribution of SAV in the littoral water near the Tiaoxi River is likely associated with the turbid river plume (Dong, Qin, Gao, & Cai, 2014). Further developments should include the influence of coastal currents, wave energy, and bathymetry, determined by numerical modeling, to generate a complete assessment of the littoral areas exposed to the Tiaoxi River turbid plume.

5. Conclusions

To examine the spatio-temporal variations of the Tiaoxi River plume and determine the effects of rainfall and wind on the plume, we used 48 250 m MODIS images acquired during 20 heavy rainfall events in Lake Taihu from 2004 to 2013. The heavy rainfall events caused a significant river plume and the input of a large amount of TSM, effects that have been ignored in previous studies on shallow large Lake Taihu. The area of the river plume was highly significantly correlated with the amount of the heavy rainfall, indicating that the rainfall amount and the attendant river discharge were determining factors for the river plume. These results confirmed that optical remote sensing can be used to monitor a discharge of terrigenous and anthropogenic TSM after heavy rainfall and the subsequent development of a turbid river plume in the waters of a lake, similar to the applications of optical remote sensing in many estuaries and coastal waters following heavy

rainfall (Lahet & Stramski, 2010; Nezlin et al., 2008; Petus et al., 2010). Remote sensing imagery has increased the current knowledge of the Tiaoxi turbid river plume, thereby supporting the management and assessment of the water quality in Lake Taihu, particularly with the increase of heavy rainfall under global warming. Considering the effects of discharge, winds and currents, additional studies are needed to understand the evolution of heavy rainfall river plumes over shorter timescales in Lake Taihu, combining the higher temporal resolution of GOCI data with in situ water quality measurements and numerical modeling.

Supplementary data to this article can be found online at http://dx.doi.org/10.1016/j.rse.2015.11.020.

Acknowledgments

This study was jointly funded by the National Natural Science Foundation of China (grants 41325001, 41230744), the Key Program of Nanjing Institute of Geography and Limnology, Chinese Academy of Sciences (NIGLAS2012135003), and the Provincial Natural Science Foundation of Jiangsu of China (BK2012050). We are grateful to the three anonymous reviewers for their constructive comments and suggestions. Data in this paper are available upon request from the first author (Address: Nanjing Institute of Geography and Limnology, Chinese Academy of Sciences, 73 East Beijing Road, Nanjing 210008, P. R. China; Tel: +86-25-86882198, Fax: +86-25-57714759; Email: ylzhang@niglas.ac.cn).

References

Bai, Y., He, X., Pan, D., Chen, C. T. A., Kang, Y., Chen, X., & Cai, W. J. (2014). Summertime Changjiang River plume variation during 1998–2010. *Journal of Geophysical Research, Oceans*, *119*, 6238–6257.

Binding, C., Greenberg, T., & Bukata, R. (2012). An analysis of MODIS-derived algal and mineral turbidity in Lake Erie. *Journal of Great Lakes Research*, *38*, 107–116.

Cannizzaro, J. P., Carlson, P. R., Yarbro, L. A., & Hu, C. (2013). Optical variability along a river plume gradient: Implications for management and remote sensing. *Estuarine, Coastal and Shelf Science*, *131*, 149–161.

Chen, S., Huang, W., Chen, W., & Wang, H. (2011). Remote sensing analysis of rainstorm effects on sediment concentrations in Apalachicola Bay, USA. *Ecological Informatics*, *6*, 147–155.

Chen, Z., Hu, C., & Muller-Karger, F. (2007). Monitoring turbidity in Tampa Bay using MODIS/aqua 250-m imagery. *Remote Sensing of Environment*, *109*, 207–220.

Choi, J. -K., Park, Y. J., Lee, B. R., Eom, J., Moon, J. -E., & Ryu, J. -H. (2014). Application of the geostationary ocean color imager (GOCI) to mapping the temporal dynamics of coastal water turbidity. *Remote Sensing of Environment*, *146*, 24–35.

Chung, H., Liu, C., Chiu, Y., & Liu, J. (2014). Spatiotemporal variation of gaoping river plume observed by formosat-2 high resolution imagery. *Journal of Marine Systems*, *132*, 28–37.

Churchill, J. H., Ralph, E. A., Cates, A. M., Budd, J. W., & Urban, N. R. (2003). Observations of a negatively buoyant river plume in a large lake. *Limnology and Oceanography*, *48*, 884–894.

Coppus, R., & Imeson, A. (2002). Extreme events controlling erosion and sediment transport in a semi-arid sub-Andean valley. *Earth Surface Processes and Landforms*, *27*, 1365–1375.

Corcoran, A. A., Reifel, K. M., Jones, B. H., & Shipe, R. F. (2010). Spatiotemporal development of physical, chemical, and biological characteristics of stormwater plumes in Santa Monica Bay, California (USA). *Journal of Sea Research*, *63*, 129–142.

Dong, B., Qin, B., Gao, G., & Cai, X. (2014). Submerged macrophyte communities and the controlling factors in large, shallow Lake Taihu (China): Sediment distribution and water depth. *Journal of Great Lakes Research*, *40*, 646–655.

Feng, L., Hu, C., Chen, X., & Song, Q. (2014). Influence of the Three Gorges Dam on total suspended matters in the Yangtze Estuary and its adjacent coastal waters: Observations from MODIS. *Remote Sensing of Environment*, *140*, 779–788.

Geary, R. C. (1954). The contiguity ratio and statistical mapping. *The incorporated statistician* (pp. 115–146).

Grosse, J., Bombar, D., Doan, H. N., Nguyen, L. N., & Voss, M. (2010). The mekong river plume fuels nitrogen fixation and determines phytoplankton species distribution in the south China sea during low-and high-discharge season. *Limnology and Oceanography*, *55*, 1668–1680.

Guneroglu, A., Karsli, F., & Dihkan, M. (2013). Automatic detection of coastal plumes using landsat TM/ETM+ images. *International Journal of Remote Sensing*, *34*, 4702–4714.

He, C., Rao, Y., Howell, T., & Skafel, M. (2006). Numerical modeling of Grand River plume during unstratified period. *Water Quality Research Journal of Canada*, *41*, 16–23.

He, X., Bai, Y., Pan, D., Huang, N., Dong, X., Chen, J., ... Cui, Q. (2013). Using geostationary satellite ocean color data to map the diurnal dynamics of suspended particulate matter in coastal waters. *Remote Sensing of Environment*, *133*, 225–239.

Hu, C., Lee, Z., Ma, R., Yu, K., Li, D., & Shang, S. (2010). Moderate resolution imaging spectroradiometer (MODIS) observations of cyanobacteria blooms in Taihu Lake, China. *Journal of Geophysical Research, Oceans (1978–2012)*, *115*. http://dx.doi.org/10.1029/2009JC005511.

Hu, W., Jørgensen, S. E., & Zhang, F. (2006). A vertical-compressed three-dimensional ecological model in Lake Taihu, China. *Ecological Modelling*, *190*, 367–398.

Kannan, N., Kim, M., Hong, S. H., Jin, Y., Yim, U. H., Ha, S. Y., ... Shim, W. J. (2012). Chemical tracers, sterol biomarkers and satellite imagery in the study of a river plume ecosystem in the Yellow Sea. *Continental Shelf Research*, *33*, 29–36.

Kharin, V. V., Zwiers, F., Zhang, X., & Wehner, M. (2013). Changes in temperature and precipitation extremes in the CMIP5 ensemble. *Climatic Change*, *119*, 345–357.

Lahet, F., & Stramski, D. (2010). MODIS imagery of turbid plumes in San Diego coastal waters during rainstorm events. *Remote Sensing of Environment*, *114*, 332–344.

Lathrop, R. G., Jr., Vande Castle, J. R., & Lillesand, T. M. (1990). Monitoring river plume transport and mesoscale circulation in Green Bay, Lake Michigan, through satellite remote sensing. *Journal of Great Lakes Research*, *16*, 471–484.

Lihan, T., Saitoh, S. -I., Iida, T., Hirawake, T., & Iida, K. (2008). Satellite-measured temporal and spatial variability of the Tokachi River plume. *Estuarine, Coastal and Shelf Science*, *78*, 237–249.

Liu, J., Liang, X., Yang, J., Ye, Y., Su, M., Nie, Z., & Chen, Y. (2011). Size distribution and composition of phosphorus in the East Tiao River, China: The significant role of colloids. *Journal of Environmental Monitoring*, *13*, 2844–2850.

Liu, X., Zhang, Y., Yin, Y., Wang, M., & Qin, B. (2013). Wind and submerged aquatic vegetation influence bio-optical properties in large shallow Lake Taihu, China. *Journal of Geophysical Research – Biogeosciences*, *118*, 713–727.

McCullough, G. K., & Barber, D. (2007). The effect of suspended solids loading from the Linthipe River on light in lake Malawi. *Journal of Great Lakes Research*, *33*, 466–482.

Murphy, R., Tolhurst, T., Chapman, M., & Underwood, A. (2008). Spatial variation of chlorophyll on estuarine mudflats determined by field-based remote sensing. *Marine Ecology Progress Series*, *365*, 45–55.

Myint, S. W., Wentz, E. A., & Purkis, S. J. (2007). Employing spatial metrics in urban land-use/land-cover mapping: Comparing the getis and geary indices. *Photogrammetric Engineering & Remote Sensing*, *73*, 1403–1415.

Nezlin, N. P., & DiGiacomo, P. M. (2005). Satellite ocean color observations of stormwater runoff plumes along the San Pedro Shelf (southern California) during 1997–2003. *Continental Shelf Research*, *25*, 1692–1711.

Nezlin, N. P., DiGiacomo, P. M., Diehl, D. W., Jones, B. H., Johnson, S. C., Mengel, M. J., ... Wang, M. (2008). Stormwater plume detection by MODIS imagery in the southern California coastal ocean. *Estuarine, Coastal and Shelf Science*, *80*, 141–152.

Nezlin, N. P., DiGiacomo, P. M., Stein, E. D., & Ackerman, D. (2005). Stormwater runoff plumes observed by SeaWiFS radiometer in the Southern California Bight. *Remote Sensing of Environment*, *98*, 494–510.

O'Gorman, P. A., & Schneider, T. (2009). The physical basis for increases in precipitation extremes in simulations of 21st-century climate change. *Proceedings of the National Academy of Sciences USA*, *106*, 14773–14777.

Ondrusek, M., Stengel, E., Kinkade, C. S., Vogel, R. L., Keegstra, P., Hunter, C., & Kim, C. (2012). The development of a new optical total suspended matter algorithm for the Chesapeake Bay. *Remote Sensing of Environment*, *119*, 243–254.

Pavlac, M. M., Smith, T. T., Thomas, S. P., Makarewicz, J. C., Edwards, W. J., Pennuto, C. M., & Boyer, G. L. (2012). Assessment of phytoplankton distribution in the nearshore zone using continuous < i > in situ</i > fluorometry. *Journal of Great Lakes Research*, *38*, 78–84.

Petus, C., Chust, G., Gohin, F., Doxaran, D., Froidefond, J. -M., & Sagarminaga, Y. (2010). Estimating turbidity and total suspended matter in the Adour River plume (South Bay of Biscay) using MODIS 250-m imagery. *Continental Shelf Research*, *30*, 379–392.

Petus, C., Marieu, V., Novoa, S., Chust, G., Bruneau, N., & Froidefond, J. -M. (2014). Monitoring spatio-temporal variability of the Adour River turbid plume (Bay of Biscay, France) with MODIS 250-m imagery. *Continental Shelf Research*, *74*, 35–49.

Qian, W., Fu, J., & Yan, Z. (2007). Decrease of light rain events in summer associated with a warming environment in China during 1961–2005. *Geophysical Research Letters*, *34*.

Qin, B., Hu, W., Gao, G., Luo, L., & Zhang, J. (2004). Dynamics of sediment resuspension and the conceptual schema of nutrient release in the large shallow Lake Taihu, China. *Chinese Science Bulletin*, *49*, 54–64.

Qin, B., Xu, P., Wu, Q., Luo, L., & Zhang, Y. (2007). Environmental issues of Lake Taihu, China. *Hydrobiologia*, *581*, 3–14.

Rao, Y. R., & Schwab, D. J. (2007). Transport and mixing between the coastal and offshore waters in the Great Lakes: A review. *Journal of Great Lakes Research*, *33*, 202–218.

Shen, F., Zhou, Y., Li, J., He, Q., & Verhoef, W. (2013). Remotely sensed variability of the suspended sediment concentration and its response to decreased river discharge in the Yangtze estuary and adjacent coast. *Continental Shelf Research*, *69*, 52–61.

Shi, K., Zhang, Y., Zhu, G., Liu, X., Zhou, Y., Xu, H., & Qin, B. (2015). Long-term remote monitoring of total suspended matter concentration in Lake Taihu using 250 m MODIS-aqua data. *Remote Sensing of Environment*, *164*, 43–56.

Stocker, T. F., Dahe, Q., & Plattner, G. -K. (2013). Climate change 2013: The physical science basis. *Working Group I Contribution to the Fifth Assessment Report of the Intergovernmental Panel on Climate Change. Summary for Policymakers (IPCC, 2013)*.

Sun, D., Li, Y., Le, C., Shi, K., Huang, C., Gong, S., & Yin, B. (2013). A semi-analytical approach for detecting suspended particulate composition in complex turbid inland waters (China). *Remote Sensing of Environment*, *134*, 92–99.

Svejkovsky, J., Nezlin, N. P., Mustain, N. M., & Kum, J. B. (2010). Tracking stormwater discharge plumes and water quality of the Tijuana River with multispectral aerial imagery. *Estuarine, Coastal and Shelf Science*, *87*, 387–398.

Thomas, A. C., & Weatherbee, R. A. (2006). Satellite-measured temporal variability of the Columbia River plume. *Remote Sensing of Environment*, *100*, 167–178.

Wang, M., Shi, W., & Tang, J. (2011). Water property monitoring and assessment for China's inland Lake Taihu from MODIS-aqua measurements. *Remote Sensing of Environment*, *115*, 841–854.

Wang, S., Qian, X., Han, B. -P., Luo, L. -C., & Hamilton, D. P. (2012). Effects of local climate and hydrological conditions on the thermal regime of a reservoir at tropic of cancer, in southern China. *Water Research*, *46*, 2591–2604.

Warrick, J. A., DiGiacomo, P. M., Weisberg, S. B., Nezlin, N. P., Mengel, M., Jones, B. H., ... Farnsworth, K. L. (2007). River plume patterns and dynamics within the Southern California Bight. *Continental Shelf Research*, *27*, 2427–2448.

White, J., Fulweiler, R., Li, C., Bargu, S., Walker, N., Twilley, R., & Green, S. (2009). Mississippi River flood of 2008: Observations of a large freshwater diversion on physical, chemical, and biological characteristics of a shallow estuarine lake. *Environmental Science & Technology*, *43*, 5599–5604.

Zawada, D. G., Hu, C., Clayton, T., Chen, Z., Brock, J. C., & Muller-Karger, F. E. (2007). Remote sensing of particle backscattering in Chesapeake Bay: A 6-year SeaWiFS retrospective view. *Estuarine, Coastal and Shelf Science*, *73*, 792–806.

Zhang, Y., Qin, B., Zhu, G., Gao, G., Luo, L., & Chen, W. (2006). Effect of sediment resuspension on underwater light field in shallow lakes in the middle and lower reaches of the Yangtze River: A case study in Longgan Lake and Taihu Lake. *Science in China Series D*, *49*, 114–125.

Zhang, Y., Shi, K., Liu, X., Zhou, Y., & Qin, B. (2014). Lake topography and wind waves determining seasonal-spatial dynamics of total suspended matter in turbid Lake Taihu, China: Assessment using long-term high-resolution MERIS data. *PloS One*, *9*, e98055.

Zhang, Y., Zhang, B., Ma, R., Feng, S., & Le, C. (2007). Optically active substances and their contributions to the underwater light climate in lake taihu, a large shallow lake in China. *Fundamental and Applied Limnology*, *170*, 11–19.

Zhu, M., Zhu, G., Nurminen, L., Wu, T., Deng, J., Zhang, Y., ... Ventelä, A. -M. (2015). The influence of macrophytes on sediment resuspension and the effect of associated nutrients in a shallow and large lake (Lake Taihu, China). *PloS One*, *10*, e0127915.

Supplementary Material

Table S1 Wind speed and wind direction before, during and after heavy rainfall

Event	Year	S	D	S	D	S	D	S	D	S	D	S	D	S	D	S	D	S	D	S	D	S	D
1	2004	Jun. 21		Jun. 22		Jun. 23		Jun. 24		Jun. 25		Jun. 26		Jun. 27		Jun. 28							
		2.0	W	1.8	SE	2.4	SE	2.0	NNE	1.2	SE	1.8	SSW	2.1	ESE	2.1	ESE						
2	2004	Sep. 12		Sep. 13		Sep. 14		Sep. 15		Sep. 16		Sep. 17											
		2.6	N	2.4	NNE	2.4	E	1.7	SE	1.6	ESE	1.7	ESE										
3	2005	Jul. 18		Jul. 19		Jul. 20		Jul. 21		Jul. 22		Jul. 23		Jul. 24									
		4.2	E	4.6	E	4.2	SE	3.9	ESE	4.2	SE	2.5	ESE	2.6	ESE								
4	2005	Sep. 9		Sep. 10		Sep. 11		Sep. 12		Sep. 13		Sep. 14		Sep. 15		Sep. 16		Sep. 17					
		1.5	NNE	1.5	E	3.2	NE	4.5	NE	0.4	NW	2.6	ESE	2.2	ESE	2.5	ESE	1.9	ESE				
5	2006	Jul. 22		Jul. 23		Jul. 24		Jul. 25		Jul. 26		Jul. 27		Jul. 28		Jul. 29							
		1.5	N	1.9	N	1.5	ESE	2.1	E	3.6	SE	2.7	SSE	2.7	SSE	1.8	ESE						
6	2007	Mar. 12		Mar. 13		Mar. 14		Mar. 15		Mar. 16		Mar. 17		Mar. 18		Mar. 19		Mar. 20					
		2.3	ESE	1.9	ESE	2.8	ESE	2.2	WNW	2.4	NE	2.3	N	1.5	ENE	1.2	N	1.6	WSW				
7	2007	Oct. 3		Oct. 4		Oct. 5		Oct. 6		Oct. 7		Oct. 8		Oct. 9		Oct. 10		Oct. 11					
		3.3	ESE	3.0	SE	2.3	SE	2.1	N	5.2	NNE	6.8	NNE	4.2	N	1.9	NNW	1.7	N				
8	2008	Jun. 4		Jun. 5		Jun. 6		Jun. 7		Jun. 8		Jun. 9		Jun. 10		Jun. 11		Jun. 12					
		5.5	WNW	2.0	NW	3.2	SE	1.6	SSW	1.8	SSW	1.5	ESE	1.7	E	2.3	NNE	3.6	SE				
9	2008	Nov. 3		Nov. 4		Nov. 5		Nov. 6		Nov. 7		Nov. 8		Nov. 9		Nov. 10		Nov. 11		Nov. 12		Nov. 13	
		1.4	WNW	1.9	ESE	1.1	WNW	1.6	NNW	2.7	NNE	4.6	NNE	4.0	N	3.2	N	3.1	WNW	2.1	WNW	1.4	S
10	2009	Mar. 31		Apr. 1		Apr. 2		Apr. 3		Apr. 4		Apr. 5		Apr. 6		Apr. 7		Apr. 8		Apr. 9			
		2.6	NNE	3.7	NNE	3.8	SE	1.6	ESE	1.8	N	1.9	NE	1.9	ESE	2.5	SE	2.4	NE	2.4	ESE		
11	2010	Apr. 8		Apr. 9		Apr. 10		Apr. 11		Apr. 12		Apr. 13		Apr. 14		Apr. 15		Apr. 16					
		4.0	SE	2.9	SE	2.3	ESE	3.0	ENE	3.1	NNW	2.5	NNE	3.6	ENE	2.1	NE	2.5	SE				

12	2010	Jul. 3		Jul. 4		Jul. 5		Jul. 6		Jul. 7																	
		1.0	WNW	2.2	NNW	2.3	WNW	1.4	S	2.0	SE	1.0															
13	2010	Oct. 8		Oct. 9		Oct. 10		Oct. 11		Oct. 12		Oct. 13		Oct. 14		Oct. 15		Oct. 16		Oct. 17							
		2.1	ENE	1.6	NE	3.1	ESE	2.3	WNW	2.0	NE	1.7	ENE	1.6	NW	2.0	NW	1.3	SE	1.3	ENE						
14	2011	Jun. 2		Jun. 3		Jun. 4		Jun. 5		Jun. 6		Jun. 7		Jun. 8													
		1.9	ESE	2.3	S	0.9	ESE	2.3	NE	2.4	E	2.1	ENE	1.5	SSE												
15	2011	Aug. 23		Aug. 24		Aug. 25		Aug. 26		Aug. 27		Aug. 28		Aug. 29		Aug. 30		Aug. 31		Sep. 1		Sep. 2					
		2.8	WNW	2.8	NNE	2.0	NE	2.5	ENE	2.5	ESE	1.7	SE	2.2	SE	2.4	NE	3.8	ENE	1.8	ENE	1.8	N				
		Sep. 3		Sep. 4																							
		2.0	N	2.8	NNW																						
16	2012	May. 4		May. 5		May. 6		May. 7		May. 8		May. 9		May. 10		May. 11											
		1.5	E	1.4	WNW	1.6	NW	1.9	SE	2.6	S	2.3	NNE	3.2	ESE	3.8	ESE										
17	2012	Jun. 14		Jun. 15		Jun. 16		Jun. 17		Jun. 18		Jun. 19		Jun. 20		Jun. 21											
		4.1	ESE	2.7	ESE	2.4	SE	2.6	ESE	1.0	SE	1.2	NNE	2.5	E	2.9	ESE										
18	2012	Aug. 6		Aug. 7		Aug. 8		Aug. 9		Aug. 10		Aug. 11		Aug. 12		Aug. 13		Aug. 14									
		3.8	NNE	4.5	N	9.0	NNE	4.5	ESE	4.0	E	2.4	S	1.4	SE	1.1	NE	0.9	WNW								
19	2013	May. 13		May. 14		May. 15		May. 16		May. 17		May. 18		May. 19													
		2.0	ESE	2.9	ESE	3.0	ENE	3.6	E	1.9	E	2.0	WNW	3.3	WNW												
20	2013	Oct. 3		Oct. 4		Oct. 5		Oct. 6		Oct. 7		Oct. 8		Oct. 9		Oct. 10		Oct. 11		Oct. 12		Oct. 13					
		2.2	NNE	1.7	ENE	2.3	N	5.4	N	6.3	NNE	5.0	NNE	1.2	WNW	1.5	ENE	2.5	ENE	2.9	SE	3.1	SE				
		Oct. 14		Oct. 15		Oct. 16		Oct. 17		Oct. 18		Oct. 19		Oct. 20		Oct. 21		Oct. 22		Oct. 23							
		2.9	S	4.9	NNE	2.9	NNW	0.9	N	1.0	ENE	0.9	WNW	1.8	NNE	2.1	NNE	1.8	WNW	1.6	N						

S: daily average wind speed; D: wind direction of daily maximal wind speed.

For 14 events with the available MODIS images before the heavy rainfall event, wind speed and direction data are provided from the antecedent one day of the first MODIS image to the final MODIS images day. For other 6 heavy rainfall events, wind speed and direction data are provided from the antecedent one day of the rainfall event to the final available MODIS images day after the heavy rainfall event.